Available online www.jocpr.com

Journal of Chemical and Pharmaceutical Research, 2016, 8(5):689-706

Research Article

ISSN : 0975-7384
CODEN(USA) : JCPRC5

Numerical viscous heating effects in renal artery stenosis under peristaltic wall motions

A. J. Keikha[1] and M. Y. Abdollahzadeh Jamalabadi[2*]

[1] *Department of Mechanical, Chabahar Maritime University, Chabahar 99717-56499, Iran*
[2]*Robotics and Energy Engineering, Dongguk University-Seoul Seoul, 04620, Korea*

ABSTRACT

Renal artery stenosis is a narrowing of arteries that carry blood to one or both of the kidneys. Most often seen in older people with atherosclerosis (hardening of the arteries), renal artery stenosis can worsen over time and often leads to hypertension (high blood pressure) and kidney damage. The body senses less blood reaching the kidneys and misinterprets that as the body having low blood pressure. This signals the release of hormones from the kidney that lead to an increase in blood pressure. Over time, renal artery stenosis can lead to kidney failure. In this study, the effects of viscous heating in renal artery stenosis under peristaltic wall motions were investigated. Renal artery stenosis usually does not cause any specific symptoms. Sometimes, the first sign of renal artery stenosis is high blood pressure that is extremely hard to control, along with worsening of previously well-controlled high blood pressure, or elevated blood pressure that affects other organs in the body.

Keywords: Renal artery stenosis, viscous heating, peristaltic motions, Fluid solid interaction

---

INTRODUCTION

Renal artery stenosis is the narrowing of one or both of the renal arteries, most often caused by atherosclerosis or fibromuscular dysplasia. This narrowing of the renal artery can impede blood flow to the target kidney, resulting in renovascular hypertension – a secondary type of high blood pressure. Possible complications of renal artery stenosis are chronic kidney disease and coronary artery disease [1].Most cases of renal artery stenosis are asymptomatic, and the main problem is high blood pressure that cannot be controlled with medication [2]. Decreased kidney function may develop if both kidneys do not receive adequate blood flow, furthermore some people with renal artery stenosis present with episodes of flash pulmonary edema [3].Renal artery stenosis is most often caused by atherosclerosis which causes the renal arteries to harden and narrow due to the build-up of plaque. This accounts for about 90% of cases with most of the rest due to fibromuscular dysplasia [4].Fibromuscular dysplasia is the predominant cause in young patients, usually females under 40 years of age[5].Fluid dampers are used in military devices [1] for shock isolation[2] and in civil structures [3]for suppressing earthquake-induced shaking [4] and wind-induced vibrations [5], among many other applications [6]. Fluid dampers work by dissipating the mechanical energy into heat [7]. This example shows the phenomenon of viscous heating and consequent temperature increase in a fluid damper [8]. Viscous heating is also important in micro flow devices, where a small cross-sectional area and large length of the device can generate significant heating and affect the fluid flow consequently [9].The structural elements of a fluid damper are relatively few [10]. Figure 1 depicts a schematic of the fluid damper modeled herein with its main components [11]: damper cylinder housing [12], piston rod [13], piston head [14], and viscous fluid in the chamber [15]. There is a small annular space between the piston head and the inside wall of the cylinder housing [16]. This acts as an effective channel for the fluid [17]. As the piston head moves back and forth inside the damper cylinder [18], fluid is forced to pass through the annular channel [19] with large shear rate [20], which leads to significant heat generation [21]. The heat is transferred in both the axial and radial directions. In the radial direction, the heat is

conducted through the cylinder house wall and convected to the air outside the damper, which is modeled using the Newton's convective cooling law [22-66].

More than 90% of the time, renal artery stenosis is caused by atherosclerosis, a process in which plaque made up of fats, cholesterol, and other materials builds up on the walls of the blood vessels, including those leading to the kidneys. More rarely, renal artery stenosis can be caused by a condition called fibromuscular dyplasia, in which the cells in the walls of the arteries undergo abnormal growth. More commonly seen in women and younger people, fibromuscular dyplasia is potentially curable.

Renal artery stenosis is often found by accident in patients who are undergoing tests for another reason. Risk factors include:

- Older age
- Being female
- Having hypertension
- Having other vascular disease (such as coronary artery disease and peripheral artery disease)
- Having chronic kidney disease
- Having diabetes
- Using tobacco
- Having an abnormal cholesterol level

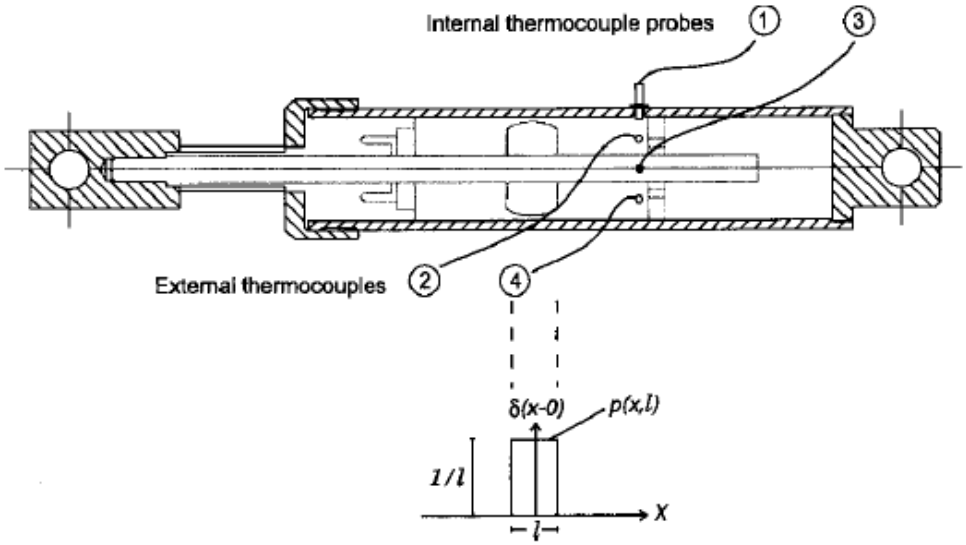

Fig.1. Top: schematic of a fluid damper that indicates the locations of the internal 1 and 3 and external thermocouples 2and 4installed on the damper tested during this study; bottom: rectangular and Dirac heat-source distributions at the piston head

Fig.2. The kidneys are two bean-shaped organs

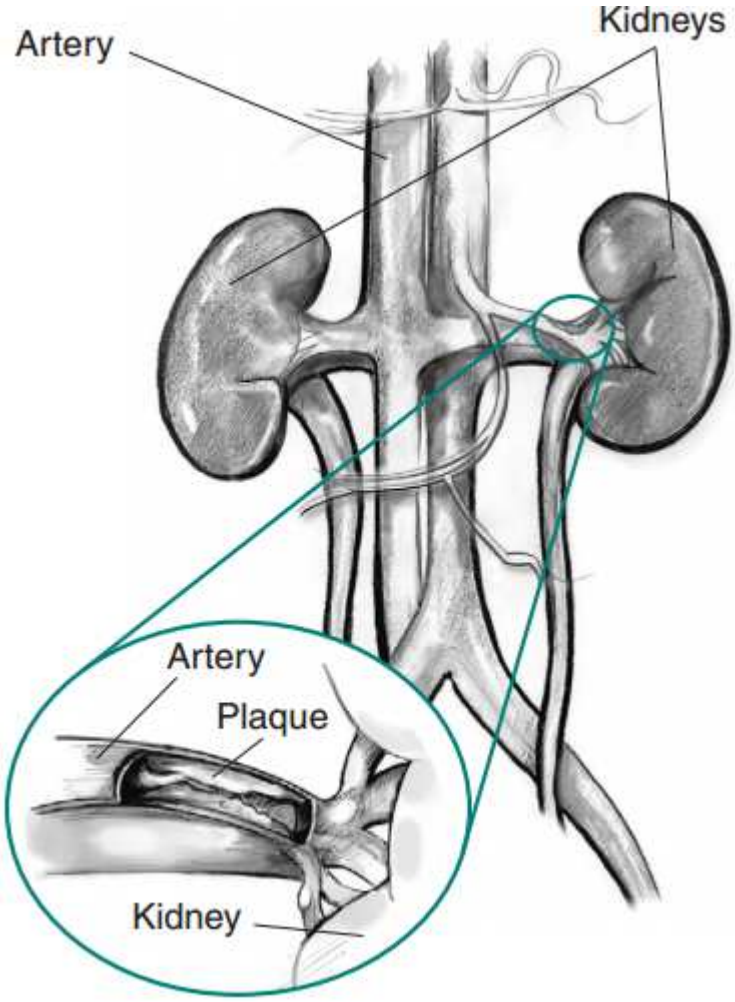

Fig.3. In most cases of RAS, plaque builds up on the inner wall of one or both renal arteries

Specialists have known for a long time that renal artery stenosis (RAS) is the major cause of renovascular hypertension and that it may account for 1-10% of the 50 million people in the United States who have hypertension. Apart from its role in the pathogenesis of hypertension, renal artery stenosis is also being increasingly recognized as an important cause of chronic renal insufficiency and end-stage renal disease. In older individuals, atherosclerosis is by far the most common etiology of renal artery stenosis.[1, 2] As the renal artery lumen progressively narrows, renal blood flow decreases. Eventually, the decreased perfusion compromises renal function and structure. With the increase in the elderly population and the possible increase in the prevalence of renal artery stenosis and ischemic nephropathy, clinicians dealing with renovascular disease (RVD) need noninvasive diagnostic tools and effective therapeutic measures to resolve the problem successfully. This article explores the natural history of this disorder, the value of a variety of invasive and noninvasive diagnostic procedures, and the consequence of allowing the artery to remain obstructed versus reversing renal artery occlusion.

EXPERIMENTAL SECTION

The goal of treatment is to reduce the risk of stroke (cerebrovascular accident). Intervention (carotid endarterectomy or carotid stenting) can cause stroke; however, where the risk of stroke from medical management alone is high, intervention may be beneficial. In selected trial participants with asymptomatic severe carotid artery stenosis, carotid endarterectomy reduces the risk of stroke in the next 5 years by 50%, though this represents a reduction in absolute incidence of all strokes or perioperative death of approximately 6%. In most centers, carotid endarterectomy is associated with a 30-day stroke or mortality rate of < 3%; some areas have higher rates [6] .

Some simplifying assumptions can be made before applying the conventional Navier–Stokes and energy equations to model the fluid flow and the heat transfer process in the micro-channel. The major assumptions are
1. The fluid is Newtonian, incompressible and with alaminar fully developed profile of velocity and a uniform inlet temperature;

2. The transport processes are considered to be steady state and bi-dimensional (throughout the microchannel the velocity and the temperature profiles are considered as fully developed);
3. Thermal radiation is neglected;
4. All channel walls are rigid and non-porous;
5. Axial thermal conduction (Pe>>1), natural convection(Gr/Re^2<< 1), and interior heat sources are neglected;
6. Fluid thermophysical properties are assumed as constant.

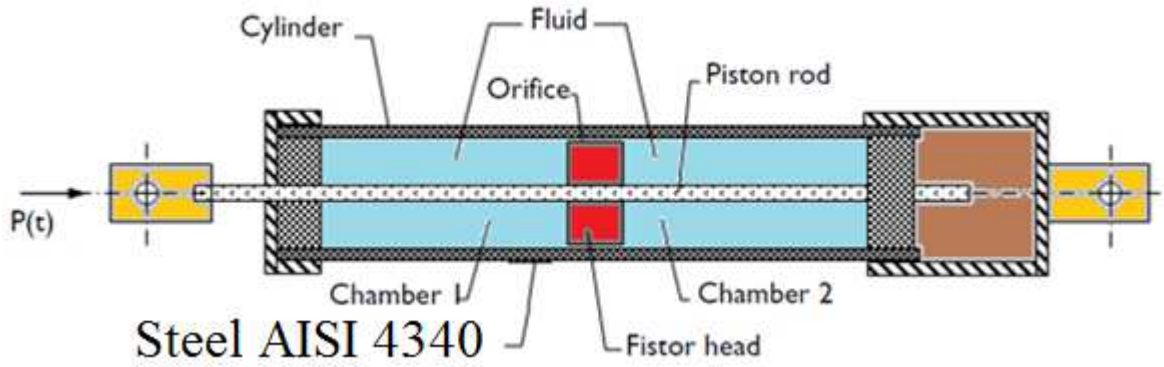

Fig.4. A sketch of a typical fluid damper with its major components

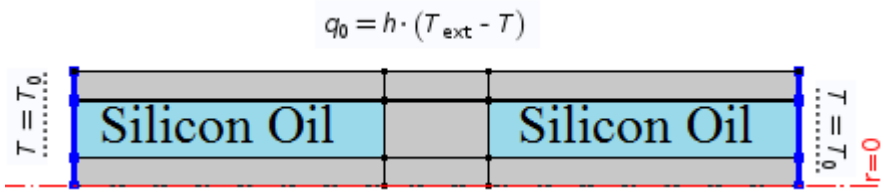

Fig.5. Boundary condition

By make use of the axially symmetric nature of the fluid damper and model it in a2D-axisymmetric geometry as shown in Figure 2. The geometric dimensions and other parameters of the damper are taken according to Ref. 1 to represent the smaller, 15 kip damper experimentally studied therein. Thus, the piston head has a diameter of 8.37 cm, the piston rod diameter is 2.83 cm, and the gap thickness is about 1/100 of the piston head diameter. The damper has the maximum stroke U0 of 0.1524 m. The damper solid parts are made of steel, and the damping fluid is silicone oil.

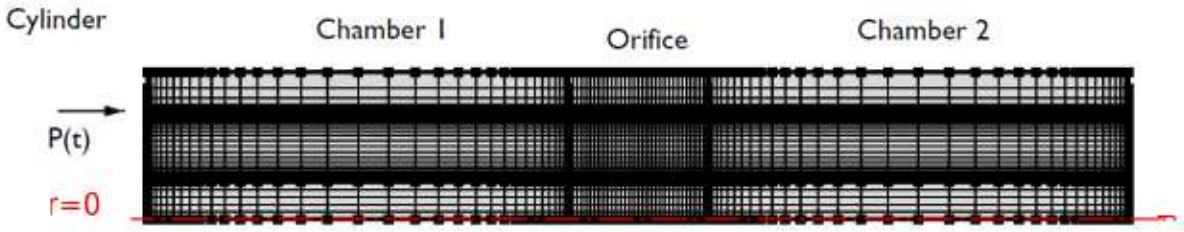

Fig.6. Geometry and mesh. The domains (from left to right) represent: piston rod, piston head and damping fluid space, the damper outer wall

The fluid flow in the fluid damper is described by the weakly compressible Navier-Stokes equations, solving for the velocity field u = (u, w) and the pressure p:

$$\rho\left(u\frac{\partial u}{\partial x}+v\frac{\partial u}{\partial y}\right)=-\frac{\partial P}{\partial x}+\mu\left(\frac{\partial^2 u}{\partial x^2}+\frac{\partial^2 u}{\partial y^2}\right)+F_x \quad (1)$$

$$\rho\left(u\frac{\partial v}{\partial x}+v\frac{\partial v}{\partial y}\right)=-\frac{\partial P}{\partial y}+\mu\left(\frac{\partial^2 v}{\partial x^2}+\frac{\partial^2 v}{\partial y^2}\right)+F_y \quad (2)$$

The density is assumed independent of the temperature, while the temperature dependence of the fluid viscosity is taken into account as the Relation between shear stress and shear rate is:

$\tau = \mu[\dot{\gamma}]$ (3)

In equation 10, the shear stress tensor is given by:

$\tau = \mu[\nabla V + (\nabla V)^{tr}]$ (4)

And the shear rate is given by:

$\dot{\gamma} = [\nabla V + (\nabla V)^{tr}]$ (5)

And viscosity is given by the power law model as follow [12]:

$\mu = m\dot{\gamma}^{n-1}$ (6)

or in a compact form

$$\nabla^2 u = -\frac{1}{\mu}\frac{dp}{d\zeta} \quad (7)$$

The reference material properties of silicone oil are used. No Slip wall boundary conditions are applied for both ends of the damper cylinder and on the inner wall of the damper cylinder house. Moving/sliding wall with the given velocity is applied on the boundaries of the piston head and on the piston rod. The conjugate heat transfer is solved both in the fluid domain and the damper cylinder house wall: heat transfer by convection and conduction in the fluid domain, heat transfer by conduction only in the solid domain, and the temperature field is continuous between the fluid and solid domains. In the fluid domain, the viscous heating is activated and pressure work can be included when the slight compressibility of the damper fluid needs to be considered:

$$\frac{dT_b}{dz} = \frac{\tilde{q}_W L^*}{Pe\,\Omega^*} + 2\frac{EcL^*}{\mathrm{Re}\,\Omega^*}\Phi^* \quad (8)$$

where the first term and second terms on the right-hand side represent the heat source from pressure work and viscous dissipation, respectively. Hence, the problem is a fully coupled fluid-thermal interaction problem. In the solid domain of the cylinder house wall, this equation reduces to conductive heat transfer equation without any heating source. The heat flux boundary condition based on the Newton's cooling law is applied on the outside boundaries of the cylinder house wall. The temperature field is continuous between the fluid and solid domains. The ends of the damper connected to the structures outside are kept at constant temperature.

In the fully developed thermal region of a heated duct the temperature profile continues to change with f but the ''relative temperature shape'' of the profile no longer changes. Using the definition of thermal fully developed region it is possible to demonstrate that, for the H1boundary condition, the energy equation can be integrated on the area of the cross-section by obtaining the following result:

$$\nabla^2\theta + \frac{\mu}{k}[\nabla u.\nabla u] = \frac{u(\xi,\eta)}{\alpha}\frac{\partial\theta}{\partial\zeta} \quad (9)$$

The piston head movement is provided as harmonic oscillations with given amplitude and frequency, $z = a_0\sin(2\pi f)$. The motion is modeled using the arbitrary Lagrangian-Eulerian (ALE) deformed mesh. The ALE method handles the dynamics of the deforming geometry and the moving boundaries with a moving grid. The Navier-Stokes equations for fluid flow and heat equations for temperature variation are formulated in these moving coordinates. Since using the definition of thermal fully developed

$$\frac{\partial\theta}{\partial\zeta} = \frac{d\theta_b}{d\zeta} = \frac{q_W + \mu\int_\Omega[\nabla u.\nabla u]d\Omega}{\rho c_p W\Omega} \quad (10)$$

Where qw is the linear heat flux to the heated wall, W is the fluid average velocity, Ω is the area of the cross-section and θ_b is the bulk temperature defined as follows:

$$\theta_b = \frac{1}{\Omega}\int_\Omega u(\xi,\eta)\theta(\xi,\eta)d\Omega \quad (11)$$

It is suitable to introduce the following dimensionless quantities:

$$x = \frac{\xi}{D_h} \tag{12}$$

$$y = \frac{\eta}{D_h} \tag{13}$$

$$z = \frac{\zeta}{L} \tag{14}$$

$$\Gamma^* = \frac{\Gamma}{D_h} \tag{15}$$

$$\Omega^* = \frac{\Omega}{D_h^2} \tag{16}$$

$$\nabla^* = D_h \nabla \tag{17}$$

$$V = \frac{u}{W} \tag{18}$$

$$T = \frac{(\theta - \theta_{in})}{\Delta\theta_{ref}} \tag{19}$$

$$L^* = \frac{L}{D_h} \tag{20}$$

$$p^* = -\frac{D_h^2}{\mu W}\frac{dp}{d\zeta} \tag{21}$$

$$Ec = \frac{W^2}{2c_p \Delta\theta_{ref}} \tag{22}$$

$$Pe = \frac{WD_h}{\alpha} = \mathrm{Re}\,\mathrm{Pr} \tag{23}$$

$$\tilde{q}_W = \frac{q_W}{k\Delta\theta_{ref}} \tag{24}$$

Consequently, the dimensionless momentum and energy balance equations are readily obtained in the following forms for the problem examined:

$$\begin{cases} \nabla^{*2}\mathrm{V} = -p^* \\ \dfrac{dT_b}{dz} = \dfrac{\tilde{q}_W L^*}{Pe\Omega^*} + 2\dfrac{EcL^*}{\mathrm{Re}\,\Omega^*}\Phi^* \end{cases} \tag{25}$$

in which the dimensionless viscous-energy-dissipation function is defined as

$$\Phi^* = \int_{\Omega^*} \left[\nabla^* V . \nabla^* V\right] d\Omega^* \tag{26}$$

The complete set of boundary conditions for the velocity distribution is thus:

$$\begin{cases} V\big|_{\Gamma^*} = 0 \\ T_b\big|_{z=0} = 0 \end{cases} \tag{27}$$

In particular, it is possible to determine the value of the Poiseuille number(the product of the Fanning friction factor for fully developed flow and the Reynolds number), using the following relation:

$$f\,\mathrm{Re} = -\frac{1}{2\Omega^*}\int_{\Omega^*}\nabla^*.(\nabla^* V)d\Omega^* = \frac{p^*}{2} \tag{28}$$

by using the properties of the Laplacian

$$\nabla^* V.\nabla^* V = -V\nabla^{*2}V + \frac{1}{2}\nabla^{*2}V^2 \tag{29}$$

By integrating Eq. (29) on the cross-section area

$$\int_{\Omega^*}\left[\nabla^* V.\nabla^* V\right]d\Omega^* = -\int_{\Omega^*} V\nabla^{*2}V d\Omega^* + \frac{1}{2}\int_{\Omega^*}\nabla^{*2}V^2 d\Omega^* \tag{30}$$

The second integral of the r.h.s. of Eq. (30) can be demonstrated to be zero:

$$\int_{\Omega^*}\nabla^{*2}V^2 d\Omega^* = \int_{\Gamma^*} n.\nabla^* V^2 d\Gamma^* = 0 \tag{31}$$

By using the Navier–Stokes equation

$$\int_{\Omega^*} V\nabla^{*2}V d\Omega^* = -p^*\int_{\Omega^*} V d\Omega^* = -p^*\Omega^* \tag{32}$$

finally

$$\Phi^* = \int_{\Omega^*}\nabla^* V.\nabla^* V d\Omega^* = 2f\,\mathrm{Re}\,\Omega^* = f\,\mathrm{Re}\frac{\Gamma^*}{2} \tag{33}$$

it is possible to show how the axial variation ofthe bulk temperature is related to the Poiseuille number:

$$\frac{dT_b}{dz} = \frac{\tilde{q}_W L^*}{Pe\Omega^*} + 4\frac{Ec}{\mathrm{Re}}\left[f\,\mathrm{Re}\,L^*\right] \tag{34}$$

By integrating Eq. (34) from the inlet to the outlet ofa long channel, where the entrance effects are negligible, one obtains the temperature rise

$$T_b(z=1) = \frac{\Delta\theta_b}{\Delta\theta_{ref}} = \frac{\tilde{q}_W L^*}{Pe\Omega^*} + 4\frac{Ec}{\mathrm{Re}}\left[f\,\mathrm{Re}\,L^*\right] \tag{35}$$

By using Eq. (35) for an adiabatic micro-channel ($q_w = 0$), the value of the dimensionless temperature at the outlet of the channel can be calculated as follows:

$$T_b(z=1) = \frac{\Delta\theta_b}{\Delta\theta_{ref}} = 4\frac{Ec}{\mathrm{Re}}\left[f\,\mathrm{Re}\,L^*\right] \tag{36}$$

As well, The temperature gradient along the channel due to the viscous heating can be expressed as follows

$$\frac{d\theta_b}{d\zeta} = \left(4\frac{Ec}{\mathrm{Re}}\left[f\,\mathrm{Re}\right]\right)\frac{\Delta\theta_{ref}}{D_h} \tag{37}$$

Morini [21] gave a fifth order polynomial approximation for calculating fRe as a function of the channel aspect ratio :

$$f\,\mathrm{Re} = \sum_{n=0}^{5} g_i\gamma^n \tag{38}$$

for two different fluids, c and d, and for a fixed value of the Reynolds number, hydraulic diameter and cross-section geometry, the temperature gradient ratio is linked to the following ratio of the fluid thermophysical properties:

$$\frac{\left(\frac{d\theta_b}{d\zeta}\right)_c}{\left(\frac{d\theta_b}{d\zeta}\right)_d} = \left(\frac{v_c}{v_d}\right)^2\left(\frac{c_{pd}}{c_{pc}}\right) \tag{39}$$

for gases the constant properties can be useful only if these two conditions are verified:

$$Ma < 0.2\frac{\Delta p}{p_{in}} < 0.05 \tag{40}$$

The theoretical value of the Poiseuille number, independent of Reynolds and experimental Poiseuille number, can be related through:

$$f\,\mathrm{Re}_{\exp} = \left(\frac{\mu(\theta_m)}{\mu(\theta_{in})}\right) f\,\mathrm{Re}_{th} \tag{41}$$

Where θ_m is the mean temperature between the inlet and the outlet. the viscous dissipation effects in adiabatic channels cannot be neglected if the following condition is satisfied:

$$4\frac{Ec}{\mathrm{Re}}\left[L^* f\,\mathrm{Re}\right] \geq 1 \tag{42}$$

If the viscous dissipation effects cause to a temperature rise of1 K between inlet and outlet, it should be considered. So

$$\left[\frac{\mu W^2 L}{\rho W c_p \theta_{ref} D_h^2}\right] \mathrm{Pr}^{-0.1} > 0.056 \tag{43}$$

If Eq. (36) can be employed to determine experimentally the value assumed by the apparent friction factor can be determined without measuring the pressure drop along the channel and just by means of temperature and flowrate measurement alone:

$$f_{app} = \frac{\Delta\theta_b}{\Delta\theta_{ref}}\left[\frac{1}{4EcL^*}\right] \tag{44}$$

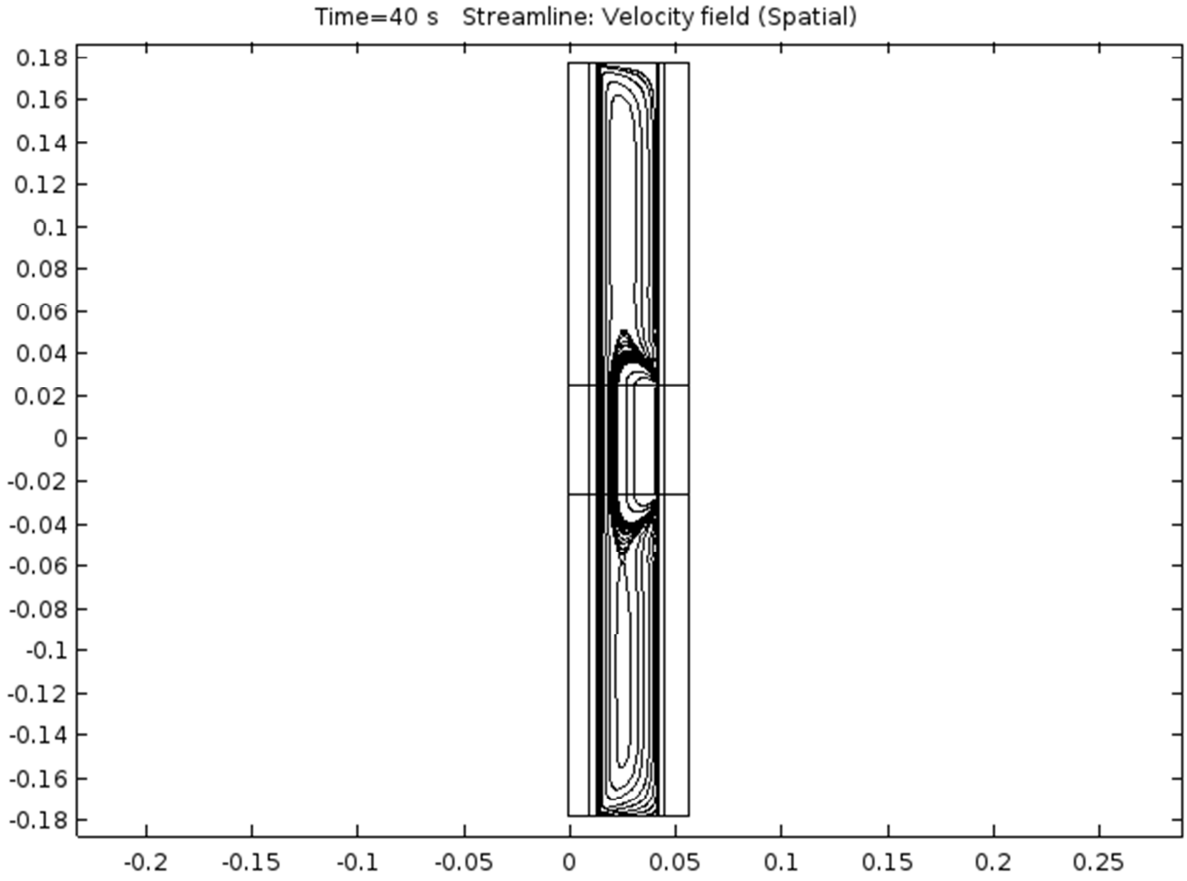

Fig.7. Streamline field in the damper at the end of simulation

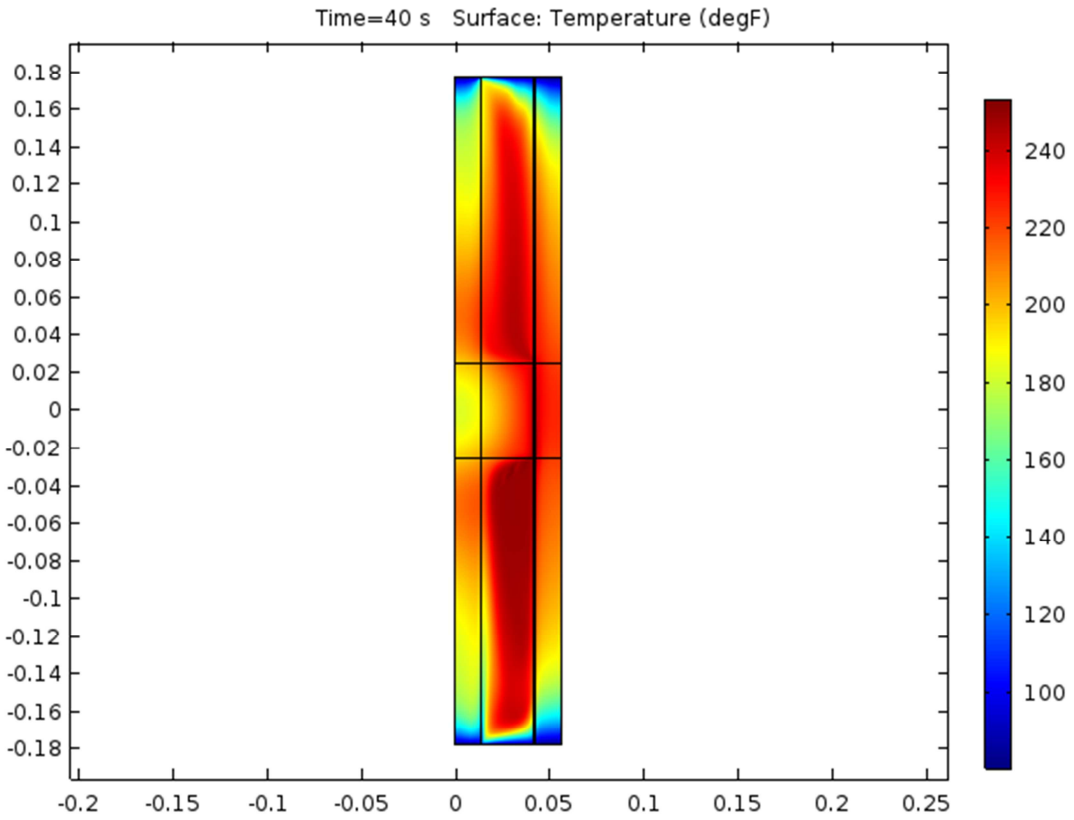

Fig.8. Temperature field in the damper at the end of simulation

The modeled loading has the amplitude of 0.127 m, and the excitation frequency is0.4 Hz. This represents the long-stroke loading experiment performed in Ref. 1. The loading time period is 40 s.

Note that the simulation results for the temperature are presented in degrees Fahrenheit for the sake of easier comparison with the experimental measurements. Figure 3 gives the temperature field in the damper at the end the loading. It also shows a typical streamline configuration for the flow induced in the damping fluid.

Figure 4 shows the temperature of the inner wall of the damper at the end-of-stroke position z = U0. This corresponds to the internal probe position under experiments performed in [1]. The simulation results show very good agreement with the experimental measurements (see Fig. 9 in [1]).

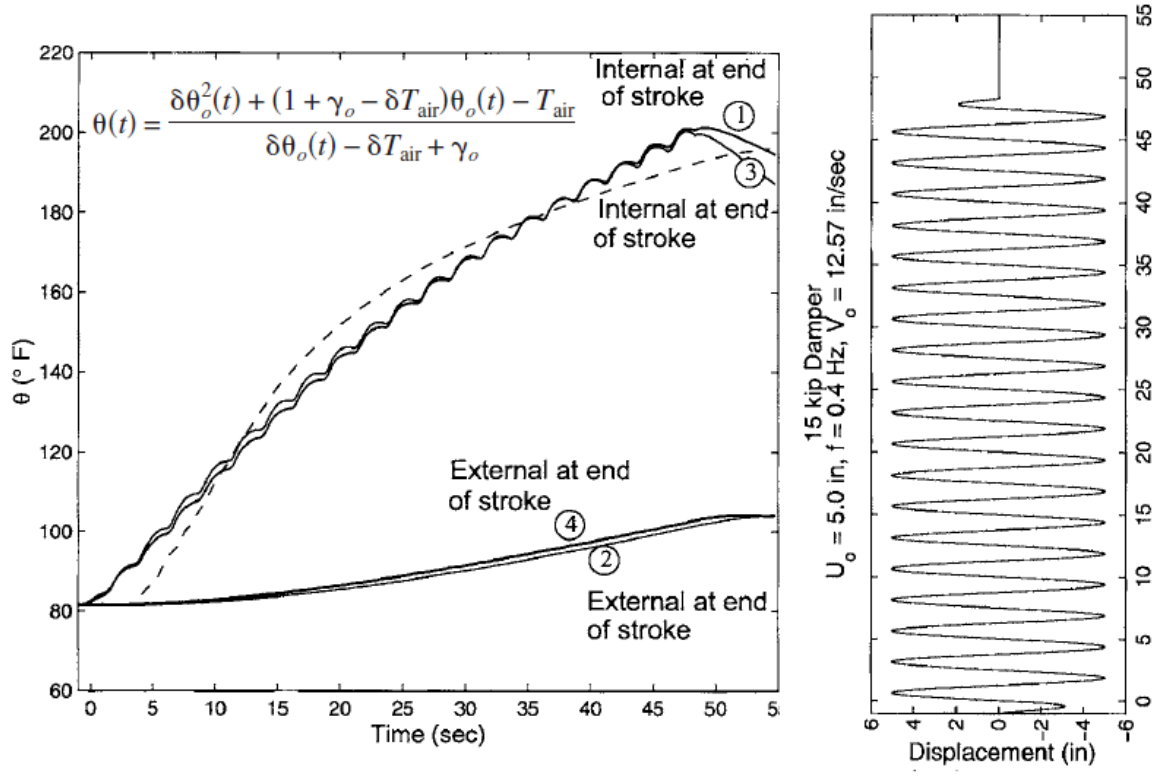

Fig.9. Temperature at the probe position

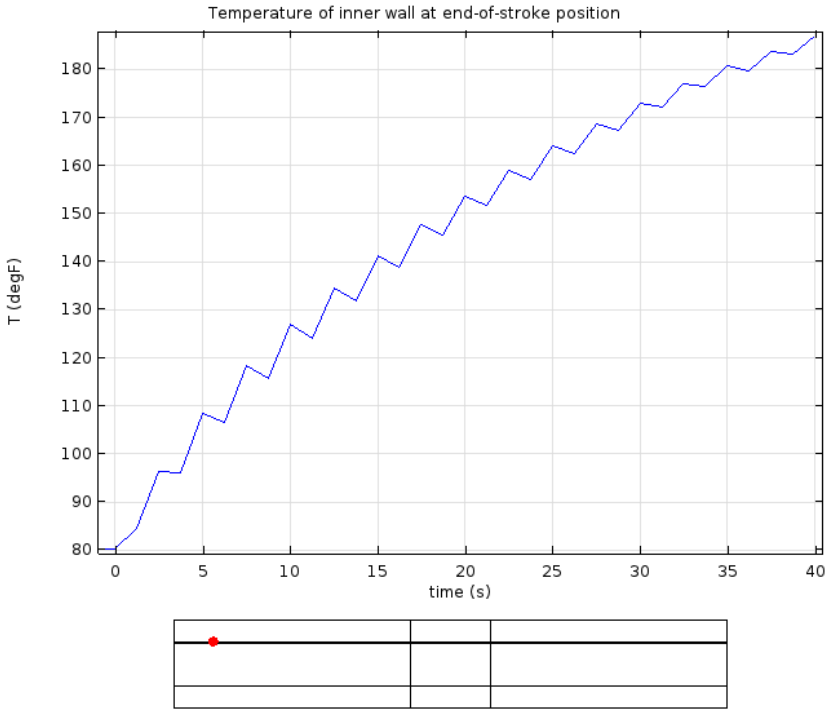

Fig.10. Temperature at the probe position

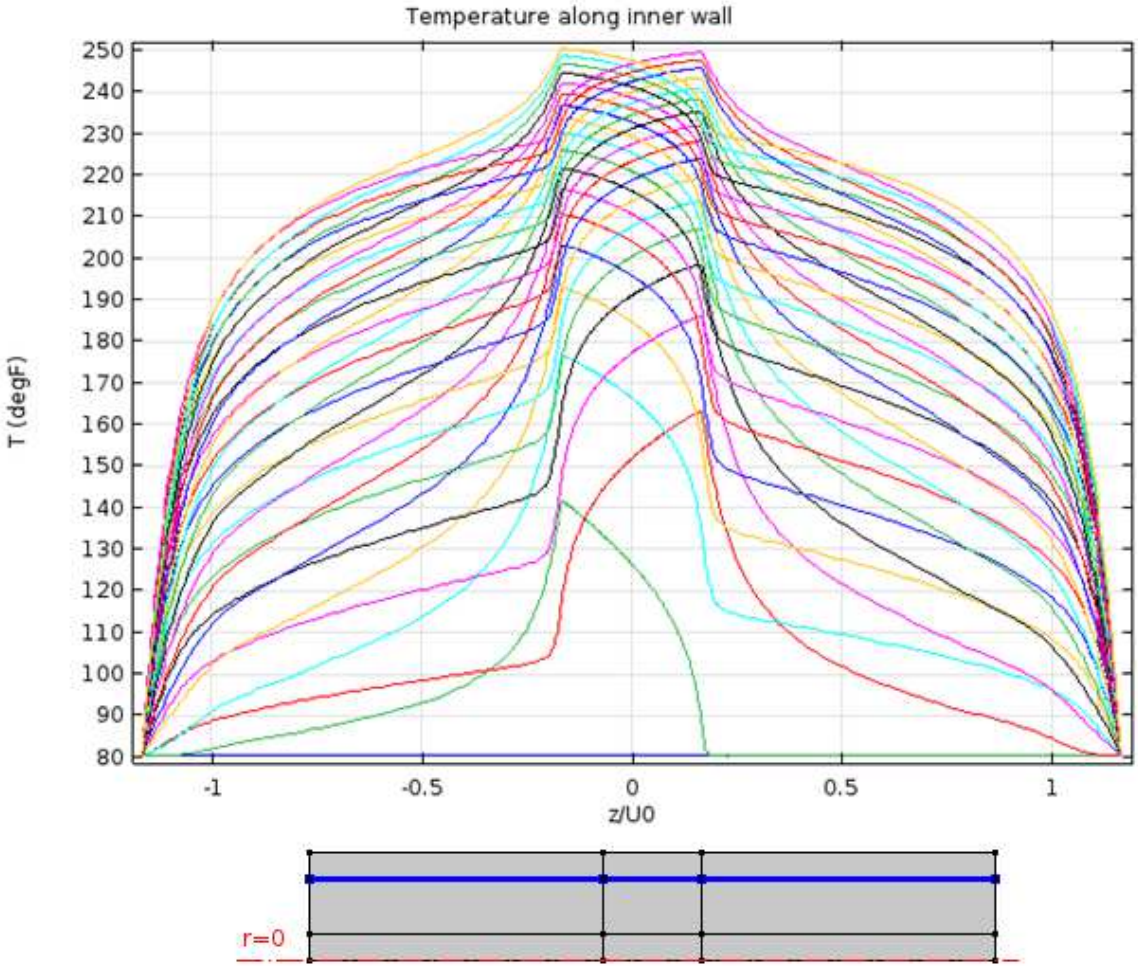

Fig.11. Temperature of the damper inner wall. T_0=80, T_{end}=240

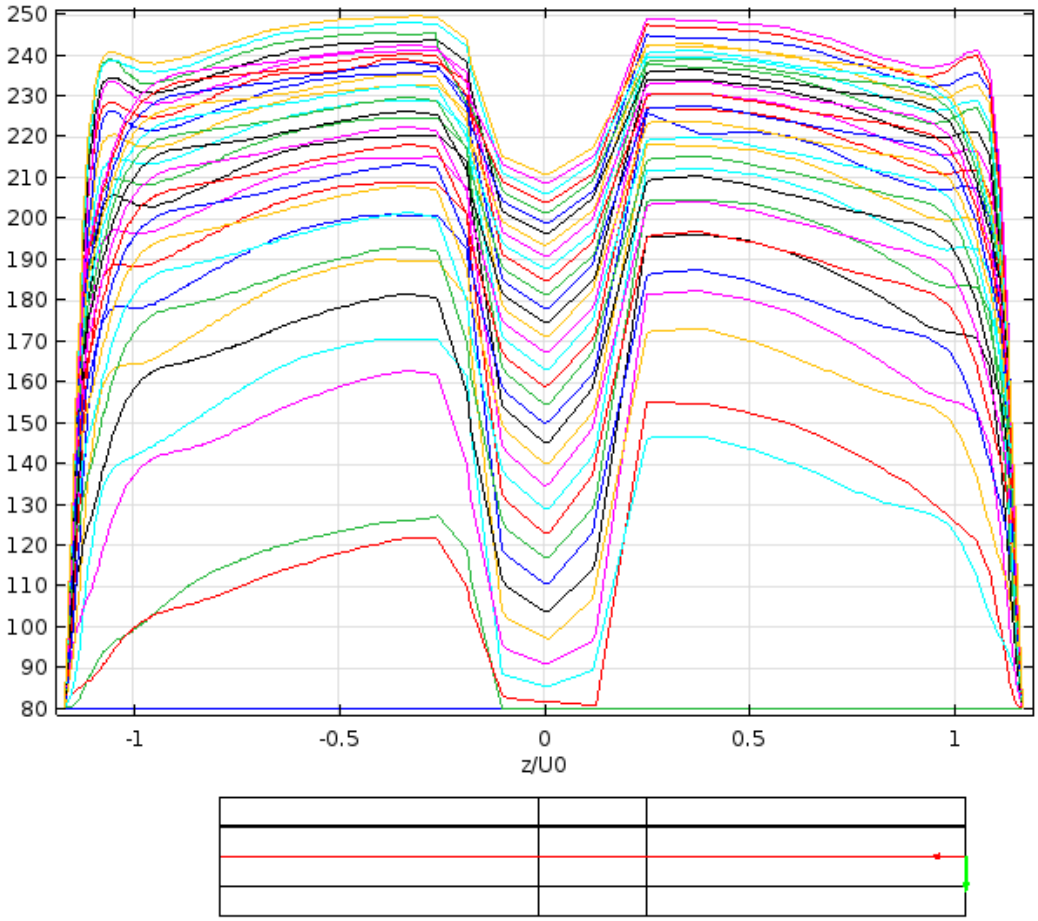

Fig.12. Temperature of the damper midline. T_0=80, T_{end}=240

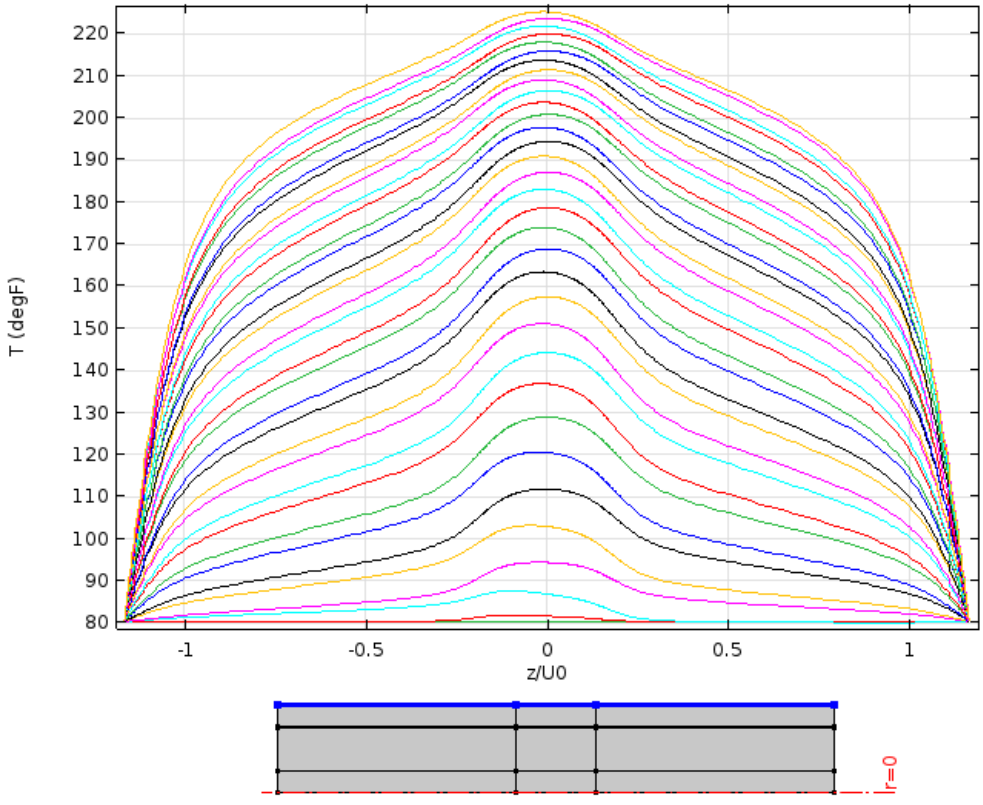

Fig.13. Temperature of the damper outer wall. T_0=80, T_{end}=240

By decompose the computational domain into several parts and mesh the domains with mapped meshes to resolve the very thin annular space. For the moving mesh you prescribe the displacement of the mesh in each domain so that their alignment remains unchanged with a zero displacement at the top and the bottom of the damper cylinder housing connecting to the high-performance seal, and the displacement equal to that of the piston head is used for the domain lined up with the piston head. This is achieved by specifying the mesh displacement field as a linear function of the deformed mesh frame coordinate and the reference (material) frame coordinate. The steel material needed for the damper solid parts is available in the built-in material library. You create a user-defined material for the silicone oil. Such damping fluids are typically characterized by the density, kinematic viscosity at the temperature 25º C, and so-called viscosity temperature coefficient, VTC = 1−(viscosity at 98.9º C)/(viscosity at 37.8º C). Using these parameters, you create the linear correlation for the dynamic viscosity given by Equation 1.

For the case of a fluid damper with force on the piston rod is *P* and radially adiabatic the one-dimensional energy equation is

$$\rho C_P \frac{D\theta(x,t)}{Dt} = k_s \frac{\partial^2 \theta(x,t)}{\partial x^2} + \frac{P(t)\dot{u}(t)}{A_P} p(x) \tag{45}$$

While in radially conduction we have

$$\rho C_P \frac{D\theta(x,t)}{Dt} + \frac{k_r 2\pi}{A_P \ln\left[1+\frac{2\varepsilon}{d_P}\right]}\left[\theta(x,t)-\theta_0(x,t)\right] = k_l \frac{\partial^2 \theta(x,t)}{\partial x^2} + \frac{P(t)\dot{u}(t)}{A_P} p(x) \tag{46}$$

the second term in Eq. (46) can be approximated with

$$\dot{q}(t) = \frac{k_s \pi d_P}{A_P \varepsilon}\left[\theta(x,t)-\theta_0(x,t)\right] \tag{47}$$

By a rectangular function distribution, with a width equal to the length of the orifice at the piston head we have

$$p(x,l) = \frac{1}{l}\left[h(x+\frac{l}{2}) - h(x-\frac{l}{2})\right] \tag{48}$$

Where*l* width of the piston head; and *h* Heaviside function of the variable *z*. The distribution is illustrated in Fig. 1. Then Solution to the Energy Equation under Small-Stroke Motions with $u_o \sin\Omega t$ is

$$\theta(x,t) = \frac{1}{4\alpha l k_s}\Delta p V_0 \int \left[\cos 2\omega_0 (t-\xi)+1\right]\left\{erfc\left[\frac{1}{2}\left(\frac{x}{l}-\frac{1}{2}\right)\frac{l\sqrt{\alpha}}{\sqrt{\xi}}\right] - erfc\left[\frac{1}{2}\left(\frac{x}{l}+\frac{1}{2}\right)\frac{l\sqrt{\alpha}}{\sqrt{\xi}}\right]\right\} d\xi \tag{49}$$

Where pressure drop across the piston head and velocity amplitude are important. But under Long-Stroke Motions Newton's law of cooling applied

$$k_s \frac{\partial \theta(x,t)}{\partial n} = h\left[T_{air} - \theta_0(x,t)\right] \tag{50}$$

where radial heat flux can be approximated with

$$-k_s \frac{\partial \theta(x,t)}{\partial n} = \frac{2k_s\left[\theta(x,t)-\theta_0(x,t)\right]}{d_p \ln\left(1+\frac{2\varepsilon}{d_P}\right)} \approx \frac{k_s\left[\theta(x,t)-\theta_0(x,t)\right]}{\varepsilon} \tag{51}$$

Substitution of the thin tube approximation

$$\frac{k_s\left[\theta(x,t)-\theta_0(x,t)\right]}{\varepsilon} = h\left[\theta_0(x,t)-T_{air}\right] \tag{52}$$

and by introducing the parameter

$$\gamma = \frac{k_s}{\varepsilon h} \tag{53}$$

can be rearranged into

$$\gamma = \frac{k_s}{\varepsilon h} = \frac{\theta_0(x,t)-T_{air}}{\theta(x,t)-\theta_0(x,t)} \tag{54}$$

Prior to loading, all the temperatures appearing in the γ ratio are equal; indicating an intermediate value γ at the initiation of loading is a constant. Subsequently, as loading proceeds, parameter γ increases at a nearly linear rate so that

$$\gamma(t) = \gamma_0 + \delta[\theta_0(t) - T_{air}] \tag{55}$$

And a more realistic law of cooling is

$$\frac{\theta_0(t) - T_{air}}{\theta(t) - \theta_0(t)} = \gamma_0 + \delta[\theta_0(t) - T_{air}] \tag{56}$$

which after rearranging terms gives

$$\theta(t) = \frac{\delta\theta_0^2(t) + (1 + \gamma_0 - \delta T_{air})\theta_0(t) - T_{air}}{\delta\theta_0(t) - \delta T_{air} + \gamma_0} \tag{57}$$

In theory, the solve for the external temperature

$$\theta_0(x.t) = \frac{1}{2\delta}\left\{A + \delta\theta(t) + \left[\delta^2\theta^2(t) + B\theta(t) + C\right]^{1/2}\right\} \tag{58}$$

RESULTS AND DISCUSSION

It is initially treated with medications, including diuretics, and medications for blood pressure control [6] .When high-grade renal artery stenosis are documented and blood pressure cannot be controlled with medication, or if renal function deteriorates, surgery may be resorted to. The most commonly used procedure is a minimally-invasive angioplasty with or without stenting. It is unclear if this approach yields better results than the use of medications alone [14]. It is a relatively safe procedure.[14] If all else fails and the kidney is thought to be worsening hypertension and revascularization with angioplasty or surgery does not work, then surgical removal of the affected kidney (nephrectomy) may significantly improve high blood pressure [15] .

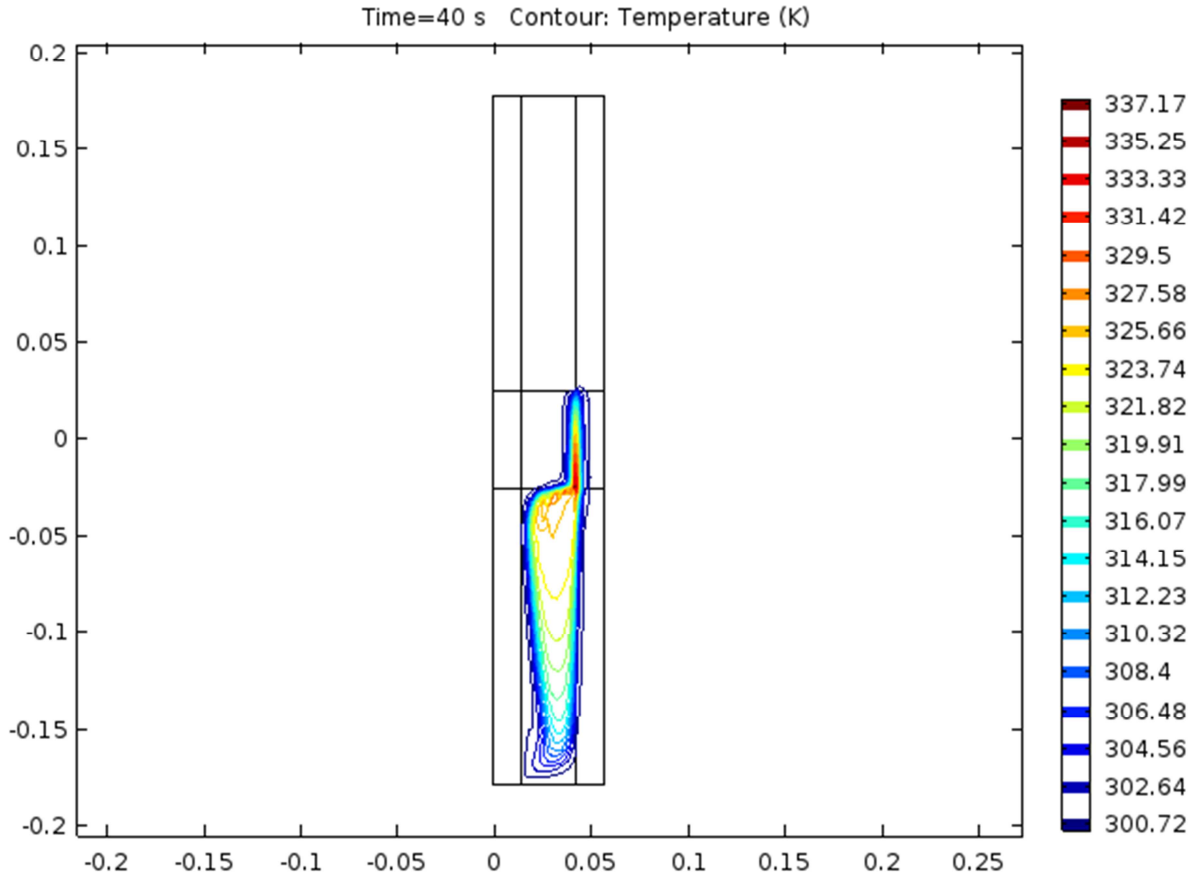

Fig.14. Temperature Contour at t=0 s

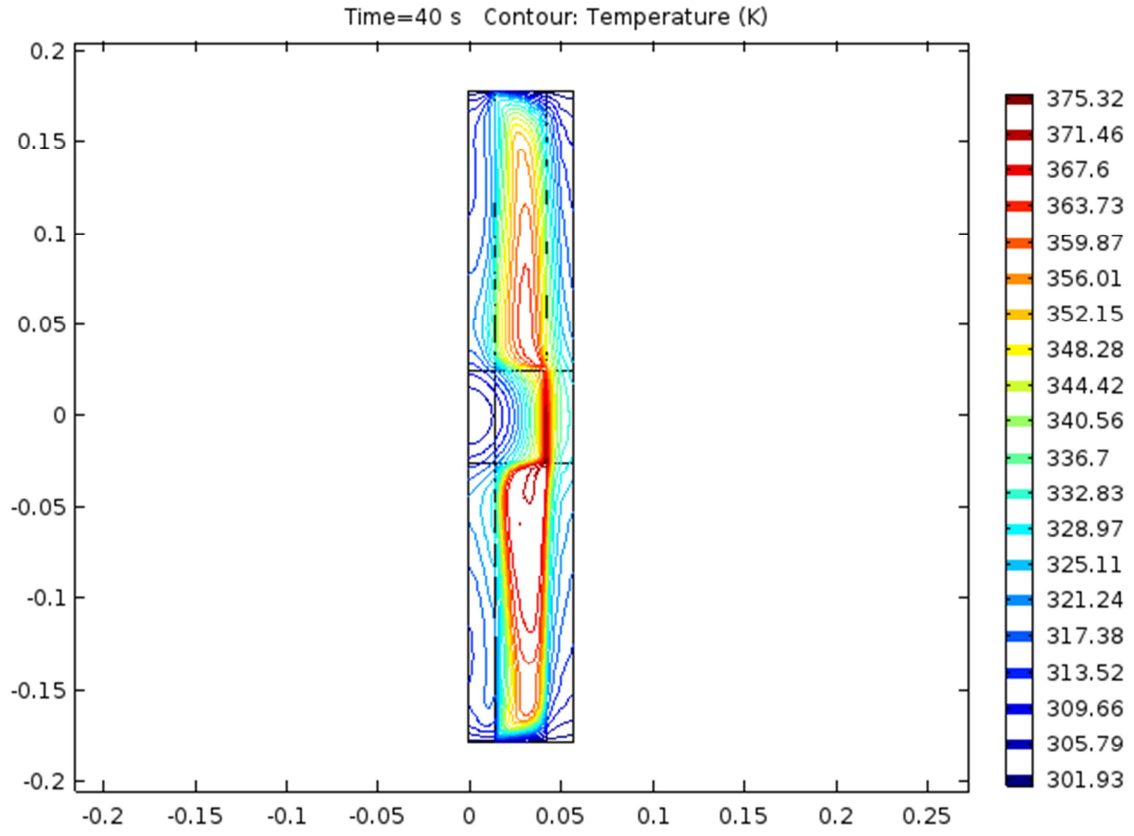

Fig.15. Temperature Contour at t=10 s

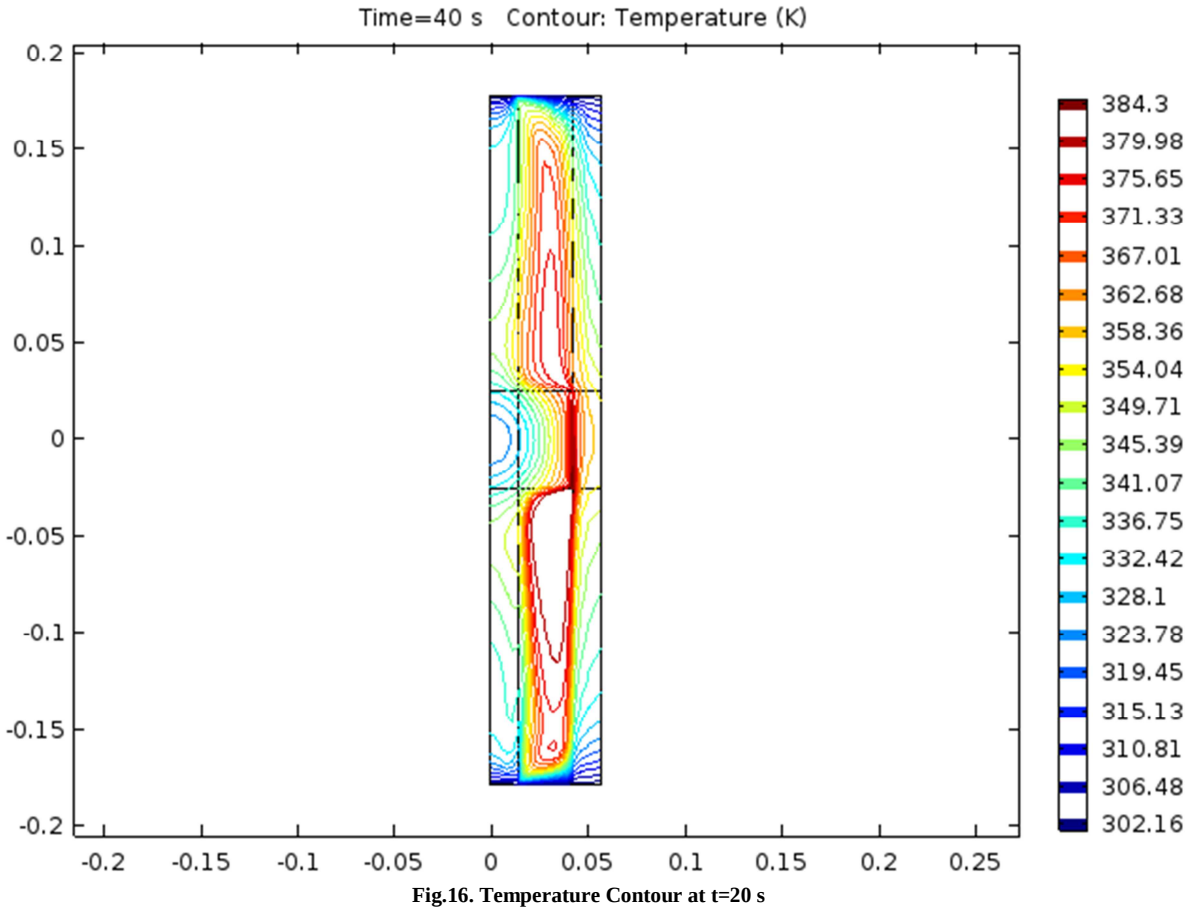

Fig.16. Temperature Contour at t=20 s

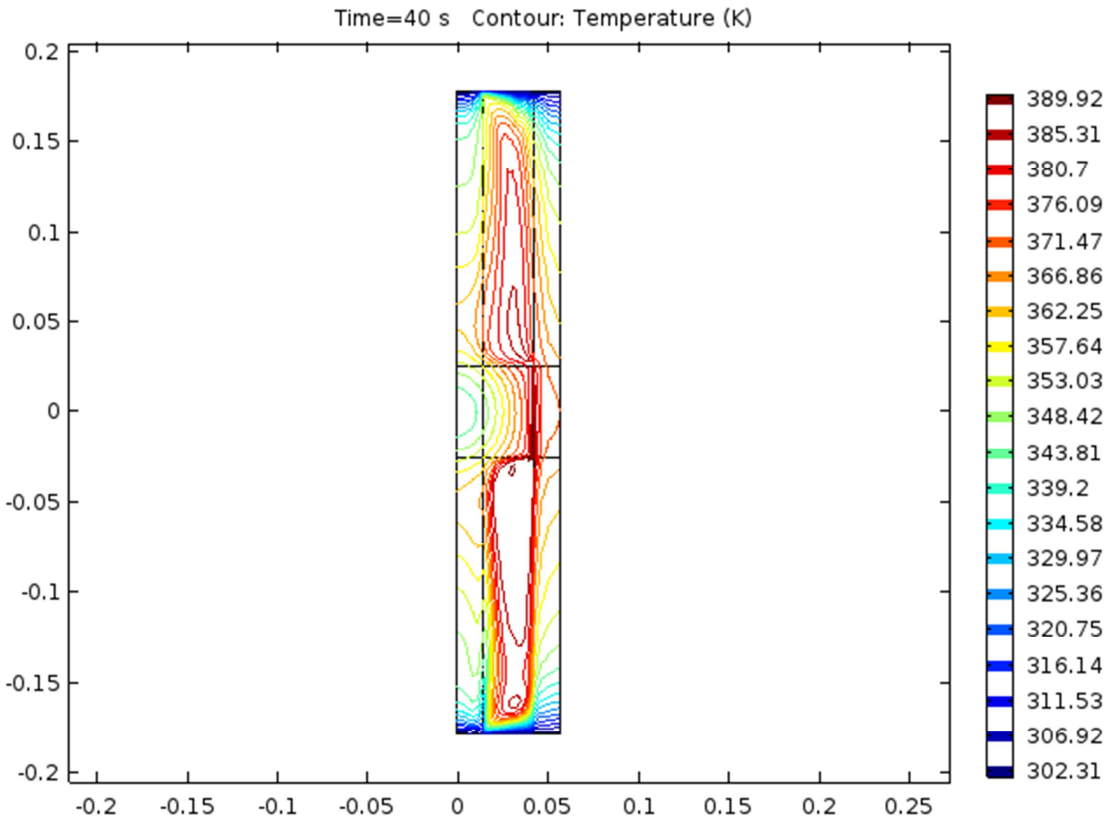

Fig.17. Temperature Contour at t=30 s

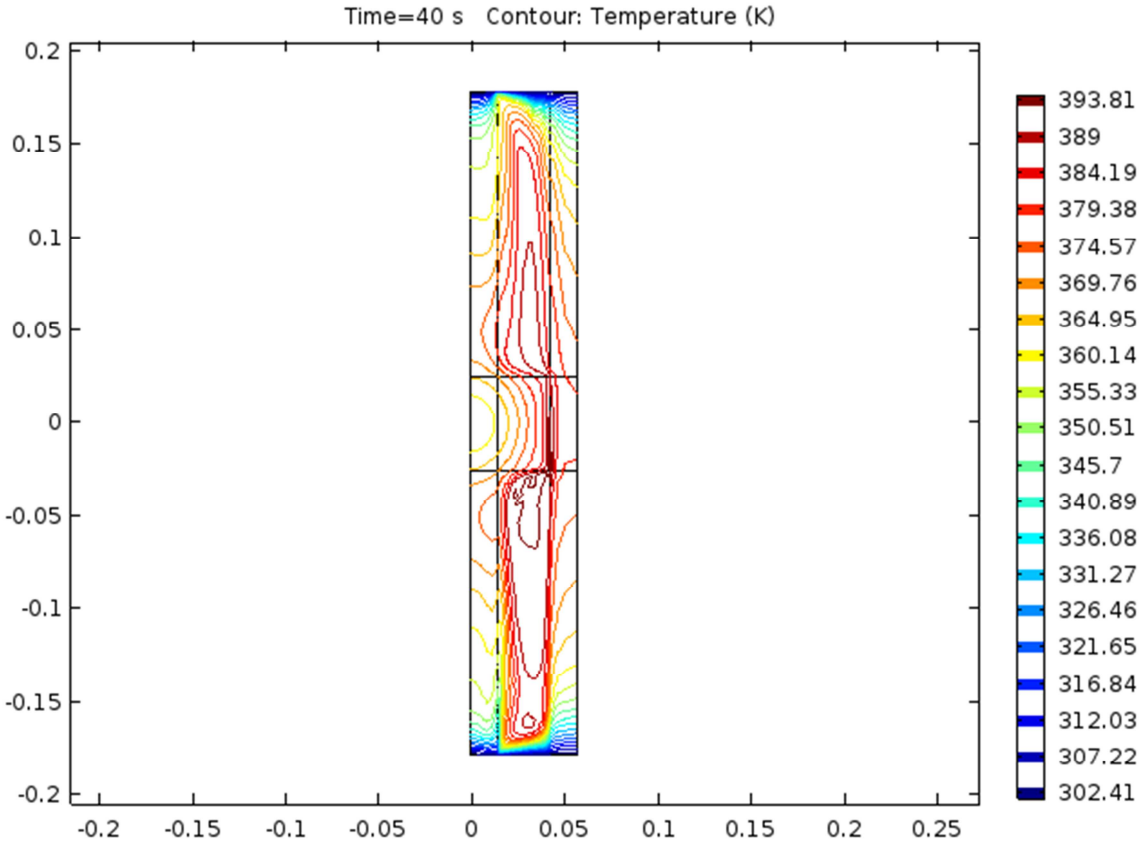

Fig.18. Temperature Contour at t=40 s

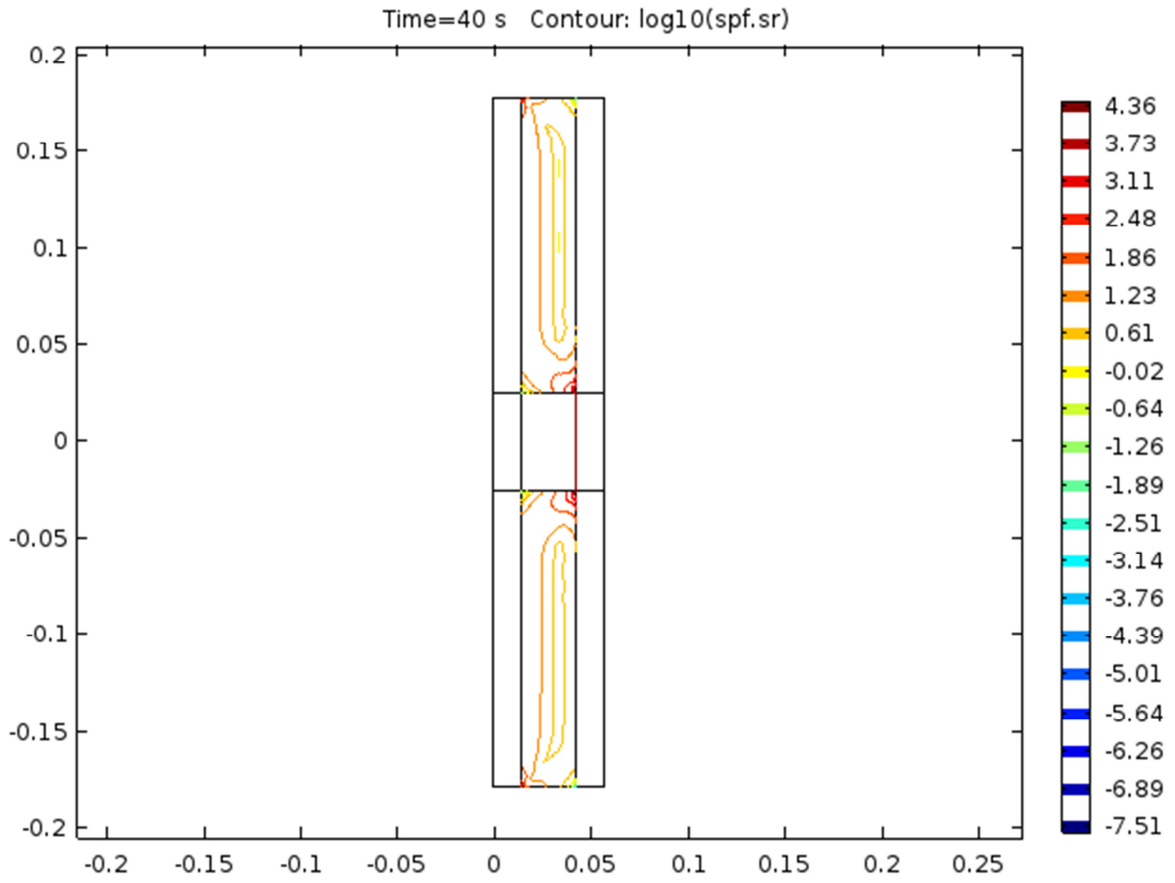

Fig.19. Shear rate at t=0 s

CONCLUSION

By taking into account the viscous heating and the consequent decrease of the fluid viscosity, it has been shown that it is possible to explain the decrease of the friction factor when the Reynolds number increases as observed by some researchers. In addition, a criterion has been presented to discern the limit for which the effect of viscous dissipation can no longer be regretted in micro-channels.

REFERENCES

[1] MY AbdollahzadehJamalabadi, *J Porous Media*, **2015**, 18(9) ,843-860.
[2] MY AbdollahzadehJamalabadi; JH Park, *ThermSci*, **2014**, 94-94
[3] MY AbdollahzadehJamalabadi, *Int J Opt Appl*, **2015**, 5 (5) , 161-167
[4] MY AbdollahzadehJamalabadi, *ChemEng Res Des*, **2015**, 102 , 407-415
[5] MY AbdollahzadehJamalabadi ; JH Park, *World App Sci Journal* , **2014**, (4)32 , 672-677
[6] MY AbdollahzadehJamalabadi; JH Park ; CY Lee, *entropy*, **2015**, 17 (2), 866-881
[7] A Shahidian; M Ghassemi; S Khorasanizade; M Abdollahzade; G Ahmadi, *IEEE Trans Magn*, **2009**, 45 (6)2667-2670
[8] MY AbdollahzadehJamalabadi, *J. Marine Sci& App*, **2014**, 13 (3) 281-290
[9] MY AbdollahzadehJamalabadi ; JH Park, *Int J. Sci Basic App Res Sci* 1 , **2014**, 421-427
[10] MY AbdollahzadehJamalabadi ; JH Park, *Open J. Fluid Dyn*, **2014**, 23 (4) 125-132
[11] MY AbdollahzadehJamalabadi;JHPark;MMRashidi ;JM Chen, *J. Hydrod Ser. B*, **2016**
[12] MY AbdollahzadehJamalabadi, *Front Heat Mass Trans*, **2015**, 6,013007
[13] M.Y. AbdollahzadehJamalabadi, *J. Fuel Cell Sci. Technol*, **2013**, 10(5) , 1039
[14] MY AbdollahzadehJamalabadi;JH Park; CY Lee, *ThermSci*, **2014**, 124-124
[15] M Jamalabadi; P Hooshmand; B Khezri ; A Radmanesh, *Ind J sci Res* 2 , **2014**, 74-81
[16] MY AbdollahzadehJamalabadi, *Mul Model Mat Struc* ,**2016**
[17] M.Y. AbdollahzadehJamalabadi, J.H.Park,C.Y. Lee, *International Journal of Applied Environmental Sciences*, **2014**, 9 (4) 1769-1781
[18] MY AbdollahzadehJamalabadi, *World App. Sci. J*. **2014**, 32 (4) 667-671

[19] MY AbdollahzadehJamalabadi, *Mid-East J. Sci Res* **2014**, 22 (4)561-574
[20] MY AbdollahzadehJamalabadi, *Mat . Perf. Char*, **2015** 20140062
[21] MS Shadloo;RPoultangari; MY AbdollahzadehJamalabadi, MM Rashidi, *Energy Conversion and Management*, **2015**,96 , 418-429
[22] MY AbdollahzadehJamalabadi; M Ghasemi; MH Hamedi ,*Int J Numer Meth Heat Fluid Flow*, **2013**, 23 (4) 649-661
[23] MY AbdollahzadehJamalabadi, *Int J Ener Mat Chem Pro*, **2016** 15, DOI:10.1615/IntJEnergeticMaterialsChemProp.2015014428
[24] MY AbdollahzadehJamalabadi, *Noise and Vibration Worldwide*, **2014**, 45 (8) 21-27
[25] MY AbdollahzadehJamalabadi, *J. King Saud UnivEngSci*, **2014**, 26 (2) 159-167
[26] MY AbdollahzadehJamalabadi ; M Ghasemi ;MH Hamedi, Proc Inst MechEng, Part C, *J. MechEngSci*, **2012** ,(226) 1302-1308
[27] M.Y. AbdollahzadehJamalabadi, *Int J EnerEng*, **2015**, 5(1) 1-8
[28] M.Y. AbdollahzadehJamalabadi, *Int J Mult Res Dev*, **2014**, (1) 5 ,1-4
[29] MY AbdollahzadehJamalabadi,SDousti, *J of Chem and Pharm Res*, **2015** (7) 12:206-218
[30] MYAbdollahzadehJamalabadi,MEbrahimi,GHomayoun,PHooshmand, *J of Chem and Pharm Res*, **2015** (7) 12 : 788-799
[31] MYAbdollahzadehJamalabadi, *Mat Per and Char* **2015** (4) 1 :1-28
[32] MYAbdollahzadehJamalabadi, *J of Niger Math Soc*, **2016**
[33] MYAbdollahzadehJamalabadi , *J of Chem and Pharm Res*, **2016**, (8) 2 : 448-469
[34] MYAbdollahzadehJamalabadi and Ovisi, M, *J of Chem and Pharm Res*, **2016**, (8) 1 : 712-728
[35] MYAbdollahzadehJamalabadi and Keikha, A., *J of Chem and Pharm Res*, **2016**, (8) 2 : 428-442
[36] P Hooshmand; MY AbdollahzadehJamalabadi; H K Balotaki; *Int Journal of Pharm Res and Allied Sci*, **2016** (5) 2 : 293-304
[37] MY AbdollahzadehJamalabadi and Keikha, A., *Ent and App Sci Let*, **2016**, 3, 2:
[38] R Patakfalvi;Dekany, *Colloid*PolymSci,**2010**, 280, 461–470.
[39] MY AbdollahzadehJamalabadi, Dousti, M; *Int J of Res and Rev in App Sci*, **2016**26,1 : 1-19
[40] MY AbdollahzadehJamalabadi, Dousti,S; *Int J of Res and Rev in App Sci*, **2015** 25,3 :55-63
[41] MY AbdollahzadehJamalabadi, *Int J of Eng and App Sci* **2015** (7) 51-21
[42] MY AbdollahzadehJamalabadi, Oveisi, M; *J of App Math and Phys*, **2016** 4 : 398-411
[42] MY AbdollahzadehJamalabadi, EFC 2013 ,**2013** 395-396
[43] PV Asharani; YL Wu; Z Gong; S Valiyaveettil, *Nanotechnology* ,**2008**, 19, 1–8.
[44] K Bilberg; MB Hovgaard; F Besenbacher; EBaatrup , *J Toxicology* ,**2012**, 293784,1-9.
[45] K Bilberg, H Malte, T Wang, E Baatrup , *Aquatic Toxicology* ,**2012**, 96,159-165.
[46] MY AbdollahzadehJamalabadi, **2015**(5) 2 :118-124
[47] P Jegadeeswaran; R Shivaraj; R Venckatesh,*Digest J Nanomaterials Biostructures* ,**2012**,7, 991 – 998.
[48] QA Pankhurst; NK T Thanh; SK Jones; and J Dobson, *J. Phys. D: Appl. Phys*., **2003**, 36, 13, 167–181.
[49] L Johannsen; J O Blanchette, *Adv. Drug Deliv*, **2004**, 56, 1649–1659.
[50] M E Davis; Z Chen; D M Shin, *Nat. Rev. Drug. Discov*, **2008**, 7, 771–782.
[51] M Arruebo; R Fernandez-Pacheco; M R Ibarra; J Santamaria, *Nano Today*, **2007**, 2, 22-32.
[52] C Alexiou; R Jurgons; C Seliger; O Brunke; H Iro; S Odenbach, ,*Anticancer Res*,**2007**, 27, 4A, 2019–2022
[53] S I Takeda; F Mishima; S Fujimoto; Y Izumi; S Nishijima, *J Magn. Magn. Mater*, **2006**,311, 367-371.
[54] K B Yesin; K lmers; B J Nelson; *Int. J. Robot. Res*, **2006**, 25, 527-536
[55] J J Abbott; O Ergeneman; M P Kummer; A M Hirt; B J Nelson, *IEEE Trans. Robot*, **2007**, 23, 1247-1252
[56] C Alexiou; D Diehl; P Henninger; H Iro; R Rockelein; W Schmidt; H Weber, *IEEE Trans. Appl. Supercond*, **2006**, 16, 1527–1530
[57] X Han; Q Cao; and L Li, *IEEE Trans. Appl. Supercond*, **2012**, 22, 3, 4401404– 4401404
[58] J-B Mathieu; S Martel, *Biomed Microdevices*, **2007**, 9, 801–808
[59] S Martel; O Felfoul; J-B Mathieu; A Chanu; S Tamaz; M Mohammadi; M Mankiewicz; N Tabatabaei, *Int. J. Rob. Res*, **2009**, 28, 9, 1169–1182
[60] H Choi; J Choi; G Jang; J Park; S Park, *Smart Mater. Struct*, **2009**, 18, 5, 055007
[61] S Jeon; G Jang; H Choi; S Park, *IEEE Trans. Magn*, **2010**,46, 6, 1943–1946
[62] H Choi; K Cha; J Choi; S Jeong; S Jeon; G Jang; J Park; S Park, *Sens. Actua. A: Phys*, **2010**, 163, 1, 410–417
[63] S Bita; MY AbdollahzadehJamalabadi, MY; M Mesbah, *J. Chem. Pharm. Res.*, **2015**, 7(11):91-98
[64] MY AbdollahzadehJamalabadi; Kim , SW ; Lee , CY ; Park, JH, *Adv in MechEng*, **2016** (8) 4 :1-10
[65] MY AbdollahzadehJamalabadi;Hooshmand, P ; Bagheri, N, KhakRah, H; Dousti, M ; *entropy*, **2016** (18) 4 :147-161
[66] MY AbdollahzadehJamalabadi, *Int J of Ener Mat and Chem Prop*, **2015** (15) 1 : 65-88